HHS Public Access

Author manuscript

J Magn Reson Imaging. Author manuscript; available in PMC 2019 April 01.

Published in final edited form as:

J Magn Reson Imaging. 2018 April ; 47(4): 1091–1098. doi:10.1002/jmri.25833.

Spatial distribution of flow and oxygenation in the cerebral venous drainage system

Jill B. De Vis, MD, PhD[1], **Hanzhang Lu, PhD**[1], **Harshan Ravi, PhD**[2], **Jeroen Hendrikse, MD, PhD**[3], and **Peiying Liu, PhD**[1]

[1]Department of Radiology, Johns Hopkins University School of Medicine, Baltimore, Maryland, USA [2]Center for Neuroscience and Regenerative Medicine, National Institutes of Health, Bethesda, MD [3]Department of Radiology, University Medical Center Utrecht, The Netherlands

Abstract

Background—The brain's arterial oxygenation, flow, and flow territories have been well investigated, but little is known about the venous system.

Purpose—The purpose of this study was to investigate the venous oxygenation and flow in the brain, and determine how they might change under challenged states.

Study type—This is a prospective study.

Subjects—Eight healthy human subjects (24-37 yrs) were studied.

Field strength/Sequence—T_2-relaxation-under-spin-tagging (TRUST) MRI and phase-contrast MRI were performed to measure venous oxygenation and venous blood flow, respectively, in the superior sagittal sinus (SSS), the straight sinus (SS), and the internal jugular veins (IJVs). Venous oxygenation was assessed at room air (0.03%CO_2, 21%O_2) and under hyperoxia (O%CO_2, 95%O_2 and 5%N_2) condition. Venous blood flow was assessed at room air and under hypercapnia (5%CO_2,21%O_2 and 74%N_2) condition. Whole-brain blood flow was also measured at the four feeding arteries of the brain using phase-contrast MRI.

Statistical tests—The changes in venous oxygenation and blood flow from room air to hyperoxia or hypercapnia conditions were tested using paired t-tests.

Results—Venous oxygenation in the SSS, the SS, and the IJVs was 61±4%, 64±4%, and 62±4% respectively at room air, and increased to 70±3% ($p<0.01$ comparing to room air), 71±5% ($p=0.59$), and 68±5% ($p<0.05$) under hyperoxic condition. The SSS, SS, and IJV drained 46±9%, 16±4%, and 79±1% of whole-brain blood flow, respectively, and this flow distribution did not change under hypercapnic condition ($p>0.5$).

Data conclusion—The results found in this paper provide insights in the venous oxygenation and venous flow distribution and its heterogeneity among different venous structures.

Corresponding author: Peiying Liu, Ph.D., Department of Radiology, Johns Hopkins University School of Medicine, 600 N. Wolfe Street, Park 324, Baltimore, MD 21287, peiying.liu@jhu.edu, Phone: 410-955-4173, Fax: 410-614-1977.

Keywords

Cerebral blood flow; Venous oxygenation; Cerebral Hemodynamics; Venous flow distribution; Venous oxygenation distribution; Brain MRI

INTRODUCTION

The brain's oxygen delivery and consumption through the vascular system represent a key process in sustaining the normal function of the brain. While the arterial oxygenation, flow, and flow territories of the brain have been extensively investigated under both baseline and challenged states (1), the brain's venous flow and oxygenation have received less attention.

Many brain diseases specifically involve the distribution of venous blood flow. In patients with venous thrombosis, venous flow, or the lack thereof, as well as the identification of collateral pathways, may help to depict those patients at risk of developing a venous stroke (2). Venous flow assessment in patients with idiopathic intracranial hypertension and dural venous sinus stenosis may be used to detect pathological cases where endovascular stent placement could be considered (3). In patients with hydrocephalus, the known interdependence of cerebrospinal fluid flow and venous blood flow may help in the assessment and therapy of these patients or could provide insight into the pathophysiology of hydrocephalus (4). Similarly, venous blood flow assessment may help to investigate the proposed hypothesis of 'venous insufficiency' in multiple sclerosis (5,6).

Knowledge of blood oxygenation in major venous branches is also of significant clinical value. In Huntington's disease (HD), decreased striatal metabolism (7), as evaluated with positron emission tomography (PET), was shown to occur even in the pre-symptomatic phase and to precede the loss of striatal volume and the onset of symptoms (8). Therefore, striatal venous oxygenation measurement may serve as a progression biomarker in HD and could be valuable for the development of disease-modifying therapies. In neonatal hypoxic-ischemic encephalopathy, brain metabolism was found to be decreased (9,10) and could thus be used to evaluate the effect of newly developed neuroprotective therapies.

Previous studies of brain oxygenation and extraction relied mainly on PET imaging, which involves radiotracers and arterial blood sampling (11). The invasiveness of PET imaging makes it less acceptable in healthy or even asymptomatic subjects. In recent years, a few new MRI approaches have been developed to assess venous oxygenation (Y_v) in large draining veins, including T_2-relaxation under spin tagging (TRUST) (12), T_2-prepared tissue relaxation with inversion recovery (T_2-TRIR) (13) and susceptometry-based techniques (14). Blood-oxygen level dependent (BOLD) techniques such as quantitative BOLD (qBOLD) (15) or calibrated BOLD (16), and susceptibility techniques such as quantitative suscetibilty mapping (QSM) (17), which allow voxel-wise oxygenation extraction mapping, were also proposed. For venous flow assessments, non-invasive methods using phase-contrast magnetic resonance imaging (PC MRI) have been developed (18,19). These novel, non-contrast techniques may accelerate the translation of venous hemodynamics assessment to clinical investigations of brain diseases (e.g., deep gray matter oxygen metabolism may be a

biomarker for HD). However, normative values for venous flow and oxygenation in major venous branches have not been established to date.

In the present study, we investigated the distribution of oxygenation and flow in the brain's venous system by measuring the oxygenation and flow in the major draining veins of the brain using TRUST MRI and PC MRI, respectively. To enhance further insight into this topic, we investigated the change in oxygenation distribution under hyperoxia condition and the change in flow distribution under hypercapnic conditions.

MATERIALS AND METHODS

Study design

The study was approved by the local Institutional Review Board. Eight subjects (four males, 24-37yrs) were studied. All subjects gave written, informed consent before participation. MR imaging was performed on a clinical 3 Tesla system (Achieva, Philips Medical Systems, Best, the Netherlands) using a quadrature body coil for transmission and a 32-channel receiver head coil. Foam padding was placed around the head to minimize motion during the MRI scan acquisition.

Each MRI session comprised three parts: 1) Measurement of oxygenation and venous blood flow at major veins, specifically, the superior sagittal sinus (SSS), the straight sinus (SS), and the internal jugular veins (IJVs), using T_2-relaxation under spin tagging (TRUST) MRI and phase-contrast (PC) MRI during room air breathing; 2) Measurement of venous oxygenation in these veins under hyperoxic (95% O2 breathing) condition; and 3) Measurement of venous blood flow in these veins under hypercapnic (5% CO2 breathing) condition. During the hyperoxic condition, we measured only venous oxygenation, because previous studies have shown minimal change in blood flow during hyperoxic challenge (20). During the hypercapnic condition, both blood flow and venous oxygenation increase, but these changes are coupled (21), so we focused only on venous blood flow during hypercapnia and did not collect venous oxygenation.

During the MRI session, the subjects were breathing through their mouth with either room air (0.03%CO_2, 21%O_2) or prepared gases (hyperoxia (O%CO_2, 95%O_2 and 5%N_2) and hypercapnia (5%CO_2,21%O_2 and 74%N_2), respectively) from a Douglas bag as earlier described (22). To restrict breathing via the nose, a tightly fitted nose clip was positioned on the subject's nose. End-tidal O_2 (EtO_2) and end-tidal CO_2 ($EtCO_2$) were monitored and recorded. Time was allotted for the subject to reach equilibrium status during normocapnia, hyperoxia, and hypercapnia before the actual MR measurements were started.

Measurements of venous oxygenation

We used the TRUST MRI (12) sequence to measure oxygenation in the main draining veins of the brain (SSS, SS, and IJVs). TRUST MRI measures the transverse relaxation rate (T_2) of pure blood and relies on the principle that the T_2 of the blood has a well-established relationship with Y_v and the hematocrit level (23). The TRUST technique magnetically labels the incoming venous blood by applying a radio-frequency (RF) pulse. Subtracting the images with and without the labeling yields an image of the pure blood signal. In addition,

flow-insensitive T_2-preparation pulses are added to incorporate T_2-weighting into the signal. The blood signal (ΔS) and the T_2-preparation duration (i.e., effective echo time (eTE)) have the following relationship:

$$\Delta S\,(eTE) = S_0 \cdot e^{eTE\cdot(\frac{1}{T_{1b}}-\frac{1}{T_{2b}})} \quad [1]$$

where S_0 is the pure blood signal without T_2-weighting, T_{1b} is the longitudinal relaxation rate of blood (assumed to be 1,624 ms (24)), and T_{2b} is blood T_2. The monoexponential fitting of ΔS and eTEs gives the T_2 value of the venous blood. The imaging parameters of the TRUST MRI sequence were as optimized in a previous study (25): repetition time (TR) 3000 ms; inversion time (TI) 1022 ms; four eTEs [1,40,80, and 160 ms] with a τCPMG of 10ms; voxel size 3.44 × 3.44 × 5 mm^3; labeling thickness 100 mm; gap 22.5 mm. For SSS and SS, we acquired three pairs of control and label images at each eTE, with a scan time of 1.2 min. For IJVs, we acquired six pairs of control and labeled images at each eTE to improve the signal-to-noise ratio (SNR) at the IJVs. Figure 1 schematically demonstrates the TRUST technique and its imaging slice positioning.

Measurement of venous flow

We used a 2D PC MRI sequence to measure venous blood flow in the major draining veins, the SSS, the SS and the IJVs. The PC MRI sequence is based on bipolar field gradients that encode flowing spins with gradient-echo acquisition using the shortest TR and TE possible. It has been validated (26) and optimized (27) previously. To understand the venous flow distribution in the venous system, the whole-brain blood flow was used as the reference. Whole-brain blood flow was calculated as the sum of influx to the brain measured at the four feeding arteries, which are the left and right internal carotid arteries (ICAs) and the left and right vertebral arteries (VAs). Thus, for each subject, and prior to PC MR imaging, three-dimensional (3D) time-of-flight (TOF) angiogram and venogram were obtained to visualize the feeding arteries and major draining veins of the brain, which is necessary for PC MRI slice-positioning. The scan parameters of the TOF angiogram and venogram were: repetition time/echo time (TR/TE) 20/3.45 ms; flip angle (FA) 18°; field-of-view (FOV); and TR/TE 25/5.76 ms; FA 20°, FOV 200 × 200 × 80 mm^3; voxel size 0.5 × 0.5 × 1 mm^3; and number of slices 80, respectively. The imaging slab of the TOF scans was centered at the level of the foramen magnum. For the angiogram, the saturation slab (60 mm thick) was positioned right above the imaging slab, while, for the venogram, the saturation slab was positioned right below the imaging slab. Imaging parameters of the PC-MRI scan were: single slice; FOV 200 × 200 × 5 mm^3; resolution 0.5; non-gated; and scan time 14.8 s. The maximum velocity encoding (V_{enc}) in the through-plane direction ranged from 30 to 60 cm/s depending on the vessel and the breathing state of the subject (Table 1). This is to achieve similar sensitivities of blood flow estimation using PC-MRI across different flow velocity of the vessels and breathing states. A lower V_{enc} was preferred to increase the signal-to-noise ratio (SNR) of voxels near the edge of the vessel, as these voxels are known to have a slower flow velocity. For voxels where the flow velocity exceeded V_{enc}, velocity aliasing correction was performed before further analysis, when needed. The PC imaging slices were positioned at the same locations on the major veins as in the TRUST MR imaging slices (Figure 1).

Positioning of the imaging slices on the feeding arteries followed that reported in a previous study (28) (see Figure 2). The imaging slices were angulated such that they were perpendicular to the targeted vessel, with the center of the vessel in the center of the imaging slice.

Data analysis

Quantification of venous oxygenation—The TRUST MRI data were processed using an in-house MATLAB script (Mathworks, Natick, MA) as described earlier (29). After motion correction, pairwise subtraction of control and label images was performed to create a difference image, which yielded a pure blood signal. Next, a preliminary ROI was manually drawn on the difference image to include the vessel of interest. Then, four voxels with the highest signals in the ROI on the difference images were chosen as the final mask for spatial averaging. Equation [1] was then fitted to the averaged blood signal to obtain a T_2 estimate, which was subsequently converted to Y_v via a calibration plot (23). For this, the hematocrit level was assumed to be 0.40 in females and 0.42 for males (29).

Quantification of venous flow—Each PC MRI scan generated three images, an anatomic image, a magnitude image (called a complex difference image), and a velocity image. The velocity image was computed from the phase difference between two scans with opposite signs of bipolar gradients. Data processing of PC MRI followed a previously reported method (28). First, as smaller V_{enc} causes phase wrapping in the voxels with a flow velocity higher than V_{enc} (usually in the center of the vessel), velocity aliasing correction (30) was performed when needed (Figure 2B and C). Next, the rater manually drew an ROI on the magnitude image by tracing the vessel wall, based on the brightness of the voxels within the vessel. While doing this, the rater was careful not to include adjacent vessels. Next, blood flow (F) was calculated by integrating the velocities (v) over the vessel area (A) within the ROIs using the following formula:

$$F = \int v dA \quad [2]$$

where v is in the unit of mm/s, A in the unit of mm^2. Therefore, the unit of F is milliliters of blood per second, i.e., blood influx per unit time.

We had two raters (PL and JD, with five and one years of experience of PC MRI ROI drawing, respectively) draw the ROIs independently to evaluate the rater-dependence of the results.

Statistical analysis

Statistical analysis was performed using SPSS (IBM SPSS Statistics for Windows, Version 21.0. Armonk, NY: IBM Corp.). Descriptive statistics were performed. The changes in oxygenation and cerebral blood flow from baseline to hyperoxia and hypercapnia, respectively, were tested using a paired-samples t-test. An ANOVA test was performed to assess changes in flow distribution from baseline to hypercapnia. A $p<0.05$ was considered

statistically significant. Inter-rater reliability of flux quantification was evaluated with the Bland-Altman method (31).

RESULTS

Venous oxygenation measurements

The measured venous oxygenation (Y_v) at room air condition was 61±4%, 64±4%, and 62±4% in the SSS, the SS, and the IJVs, respectively (Figure 3a). The SS-Y_v was significantly higher than the SSS-Y_v (p=0.0003, Figure 3A). There was a significant correlation between the SSS-Y_v and SS-Y_v (R^2=0.88, Figure 3B), and between the SSS-Y_v and the IJV-Y_v (R^2=0.65).

Under hyperoxic condition, the Y_v increased to 70±3%, 71±5%, and 68±5% in the SSS, the SS, and the IJVs, respectively ($p < 0.01$, $p = 0.59$, and $p < 0.05$).

The EtO2 and EtCO2 levels under the room air condition and hyperoxia condition are shown in Table 2.

Venous flow measurements

Mean blood flow (in ml/min) across all subjects (mean ± standard deviation (SD)) of the whole-brain and the individual draining veins of the SS, the SSS and the IJV under both room air and hypercapnic condition are shown in Table 3.

Under room air conditions the SSS, SS, and IJVs drained 46±9%, 16±4%, and 79±1% of the arterial inflow, respectively (Figure 4). We found that the venous blood drained from the cortex (i.e., flowed through the SSS) and that which drained from the deep brain structures (i.e., flowed through the SS) comprised around 62% of the whole-brain blood (i.e., total arterial inflow). Since the IJVs drain about 79% of the whole-brain blood flow, 17% of the total brain blood flow is drained through the cerebral and cerebellar veins, which drain into the venous sinuses after the sinus confluence (for instance, the vein of Labbé). Moreover, about 21% of cerebral blood was not drained by the IJVs, but via venous plexuses, which subsequently drain into the cervical veins and the external jugular veins (Figure 4).

Under hypercapnic condition, the drainage distribution did not show a significant change, and was 50±1%, 16±0.5%, and 82±1% for the SSS, SS, and IJVs, respectively (Table 3). The arterial inflow increased by 42% at hypercapnia ($p < 0.001$), while the venous drainage through the SSS, the SS, and the IJVs increased by 52%, 39%, and 49%, respectively ($p < 0.01$, $p = 0.073$, and $p < 0.01$). The relative increase in blood flow from room air to hypercapnia did not differ significantly among the investigated vessels ($p>0.5$).

The EtCO2 levels under the room air condition and hypercapnia condition are shown in Table 2.

Inter-rater reliability of the blood flow quantification

Inter-rater reliability was determined to investigate the effect of manual delineation on blood flow quantification. In the ICAs, the flux values obtained by the two raters differed by

0.22% on average, with a 95% confidence interval of −0.23 %, 0.67 %. In the VA, the inter-rater difference was 0.95%, on average, with a 95% confidence interval of −2.12 %, 4.03 %. In the SSS, the CBF values differed, on average, by 0.55%, with a confidence interval of 0.25%, 0.85%. The CBF values in the SS differed, on average, 3.43%, with a confidence interval of −3%, 9.8%. In the IJVs, the CBF values differed, on average, 1.73%, with a confidence interval of 1%, 2.5%. Our results demonstrated that there was close agreement on CBF quantification by different raters, suggesting that our CBF results have minimal rater-dependence.

DISCUSSION

In this work, we evaluated the distribution of oxygenation and flow in the venous drainage system of the brain. We provided the venous oxygenation and blood flow values as well as their distribution in major draining veins of the brain in eight normal subjects. The distribution of venous flow and oxygenation did not change under challenged states, which implies that, in normal volunteers, $EtCO_2$ and EtO_2 do not alter the distribution patterns of venous oxygenation and flow.

We found that the venous oxygenation results in the IJVs to be closely related to the results in the SSS. Therefore, if the goal is to know the whole-brain oxygen consumption, in healthy controls or in disease states without regional implications, Y_v measurements on the SSS are good indicators of whole-brain oxygenation/metabolism. This is of importance as IJV measurements require additional venogram for slice positioning, and require twice the scan duration to overcome the lower SNR at this area. Caution should be used in cases of disease conditions in which regional oxygen consumption may differ, for instance, in stroke conditions. In these cases, additional Y_v measurements on the SS and the IJVs, feasible with TRUST MRI, can be considered.

With regard to flow, hypercapnia induced similar changes on both the arterial side and venous side. The changes of blood flow due to hypercapnia challenge are often referred to as cerebrovascular reactivity (CVR), which is an important index of vascular function in the brain (32). Our results suggest that, an evaluation of only the flow in the SSS under both baseline and hypercapnia states, in contrast to the evaluation on the arterial side that requires measurements in four arterial vessels, could provide a time-efficient way to assess whole-brain cerebrovascular reactivity in healthy subjects. However, care needs to be taken in case of pathological conditions where regional vascular function could be affected.

In this paper, we applied TRUST MRI to measure the oxygenation in the SSS, the SS, and in the IJVs. Our results are comparable to the values found earlier using other T_2-based measurements. Krishnamurthy et al. found values of 59.8% and 63.5% in the SSS and SS, respectively (34). Jain et al. found values of 63%, 68%, and 65% in the SSS, the SS, and the IJVs, respectively (33) (for comparison, our values were 61%, 64%, and 62%, respectively). Similarly, those authors also found the oxygenation value in the IJVs to be closer to the oxygenation value found in the SSS than in the SS (33). This agrees with our finding that oxygenation in the IJVs is mainly driven by cortical oxygen consumption, similar to the condition in which most flow that drains through the IJVs comes from the SSS. The

consistently higher values in the SS may reflect lower oxygen metabolism in the deep tissue structures, which are drained by the SS and mainly consist of white matter. The oxygenation changes during the hyperoxic challenge in this study (Δ = +9%) closely resemble the earlier reported increase in SSS oxygenation caused by hyperoxia, as found by Xu et al. (Δ = +11%) (20). We did not note a change in oxygenation distribution from baseline to hyperoxia, which suggests that the measurements were not influenced by a subject's EtO_2, and thus, does not need to be considered. However, whether the same holds true in disease states must be confirmed. The reliability of non-invasive regional venous oxygenation measurements shows promise for the investigation of disease states. For instance, metabolism in the deep gray matter of patients with Huntington's disease was shown to decrease in the pre-symptomatic stage, and time to disease-onset could be predicted based on those measurements (8). However, for this, invasive PET measurements are necessary, which cannot be repeated frequently due to the associated radiation exposure. In addition, further research is hampered due to the fact that invasive measurements are ethically more difficult to perform on healthy control subjects. Venous oxygenation measurements of the SS could be used as a surrogate for PET metabolism measurements in the deep gray matter, and therefore, may, potentially, become a non-invasive biomarker. A similar case holds true in infants with hypoxic-ischemic encephalopathy. In those infants, the instigation of neuroprotective treatment may be based on regional venous oxygenation as a surrogate for regional brain metabolism.

We compared venous flow in the main venous sinuses to the total arterial inflow. The results found in this study are of importance as they provide reference values to which disease states can be compared. For instance, in the field of multiple sclerosis research, there has been a debate about whether absolute venous blood flow differs between patients with multiple sclerosis and healthy controls (5,6). Physiological variation in blood flow complicates the investigation and this problem may be reduced by comparing relative blood flow values. In fact, one study demonstrated differences in relative blood flow in the IJVs (35), which warrant further investigation. With the approach presented in this paper, relative blood flow through all venous sinuses can be measured relatively easily with a non-invasive and fast MRI-based method. This way, patients can undergo these measurements at the same time as their MRI scan for diagnostic work-up. This paper also presents, for the first time, venous flow distribution under challenged states. We did not find a difference in relative venous blood flow from baseline to hypercapnia in healthy controls, which suggests that a subject's $EtCO_2$ has little influence in venous flow distribution. However, whether the same holds true for pathological states still needs to be confirmed. Our absolute venous flow measurements in the SSS and in the SS are a bit higher than previously reported research. Schuchardt et al. found values of 228 ml/min in the SSS and 60 ml/min in the SS, while we found 362 and 124 ml/min (19). However, our comparison with arterial inflow does demonstrate that the values that we found are in line with what can be expected. Even more so, the relative flow through the IJVs, as reported in our study (79%), is very close to the value found by Sethi et al. (74%) (35), and we demonstrated that rater-effect did not introduce uncertainty in our flow quantification, as we found close agreement between two raters. Thus, the somewhat lower absolute flow values found in the study by Schuchardt et al. might be explained by their lower image resolution, as we did not notice an important difference in velocity

encoding (19). Interestingly, it seems to be a consistent finding that the IJVs do not drain all the arterial inflow (35). Around 20% of the brain's blood inflow seems to be drained via the venous plexuses, which subsequently drain into the cervical veins and external jugular veins. In addition, some blood fluid might drain through the brain's lymphatic system that line the venous sinuses (36). Insight into normal venous blood flow values across the different sinuses is of importance, as it has been shown earlier that deviations of normal flow could be used as outcome markers or could be used to guide treatment. For instance, based on venous flow patterns, one might be able to predict the occurrence of venous stroke in patients with venous thrombosis (2). Or, hydrocephalus patients with hemodynamically significant venous stenosis may be helped with stent placement (3). Venous flow measurements may help to unravel hydrocephalus (37), and regional venous flow measurements may help in the understanding of the pathophysiology of traumatic brain injury (38).

The strength of this study is that we applied relatively simple measurements, TRUST MRI and PC MRI, to obtain information about venous oxygenation and flow distribution. The advantage of PC MRI is that it integrates vessel ROIs obtained during several repetitions to calculate venous flow. In this way, vessel variability, especially common in venous structures that have thin, non-muscular walls and are easily compressible and distensible, is taken into account. Factors that induce variation in venous flow measurements of up to 20% are body/head position (39), respiratory state (40), and diurnal variation caused by hydration level and caffeine intake (41). Similarly, oxygenation levels have been shown to differ over the time course of a day (42). Therefore, future studies should be designed such that those variables are kept consistent over different patient populations.

The findings from the present study need to be interpreted in the context of its limitations. First, the sample size of this study (N=8) is small and only young subjects (24-37 years old) were included. A larger-scaled study with broader age range could be performed in future to establish the normative values in an age-specific manner. Second, in hyperoxia condition, we only measured venous oxygenation. Our EtCO2 recording suggested that there is a small effect of hyperventilation-induced hypocapnia. Some studies showed that this hyperventilation effect may cause a small amount of blood flow change (~7% for 100%O2) (43), but it has also been demonstrated that after accounted for the hyperventilation effect, blood flow remains constant (44). Therefore, adding additional measurement of blood flow during hyperoxia may provide more information on this topic.

In this paper, we reported the venous oxygenation and flow distribution in the major draining veins of eight healthy subjects, which could be used to define abnormal values as markers for disease or to instigate treatment. These values could also be used as a benchmark to investigate the pathophysiology of disease and to develop biomarkers. Our findings support the use of oxygenation measurements in the SSS as a surrogate for whole-brain oxygenation in healthy or disease states that affect the whole brain, but also suggest that oxygenation measurements in the SS and IJV by TRUST MRI are feasible and reliable for the assessment of regional oxygenation/metabolism, when necessary. Our blood flow results also demonstrate that cerebrovascular reactivity measurements using PC MRI can be simplified by performing a measurement solely at the SSS.

Acknowledgments

Grant Support:

This work was supported by NIH R01 AG042753 (to H.L.), NIH R01 MH084021 (to H.L.), NIH R01 AG047972 (to H.L.), NIH R21 NS095342 (to H.L.), NIH R21 NS085634 (to P.L.), Netherlands Organization for Scientific Research (NWO) grant n°91712322 (J.H.), and European Research Council grant agreement n°637024 (J.H.).

References

1. Hendrikse J, van der Grond J, Lu H, van Zijl PC, Golay X. Flow Territory Mapping of the Cerebral Arteries With Regional Perfusion MRI. Stroke. 2004; 35:882–887. [PubMed: 14988567]
2. Schuchardt F, Hennemuth A, Schroeder L, et al. Acute Cerebral Venous Thrombosis: Three-Dimensional Visualization and Quantification of Hemodynamic Alterations Using 4-Dimensional Flow Magnetic Resonance Imaging. Stroke. 2017; 48:671–677. [PubMed: 28179559]
3. Levitt MR, McGah PM, Moon K, et al. Computational Modeling of Venous Sinus Stenosis in Idiopathic Intracranial Hypertension. AJNR Am J Neuroradiol. 2016; 37:1876–1882.
4. Dreha-Kulaczewski S, Joseph AA, Merboldt K-D, Ludwig HC, Gartner J, Frahm J. Identification of the Upward Movement of Human CSF In Vivo and its Relation to the Brain Venous System. J Neurosci. 2017; 37:2395–2402. [PubMed: 28137972]
5. Rodger IW, Dilar D, Dwyer J, et al. Evidence against the involvement of chronic cerebrospinal venous abnormalities in multiple sclerosis. A case-control study. PLoS One. 2013; 8:e72495. [PubMed: 23967312]
6. Schelling F. Damaging venous reflux into the skull or spine: relevance to multiple sclerosis. Med Hypotheses. 1986; 21:141–8. [PubMed: 3641027]
7. Hayden MR, Martin WR, Stoessl AJ, et al. Positron emission tomography in the early diagnosis of Huntington's disease. Neurology. 1986; 36:888–94. [PubMed: 2940474]
8. López-Mora DA, Camacho V, Pérez-Pérez J, et al. Striatal hypometabolism in premanifest and manifest Huntington's disease patients. Eur J Nucl Med Mol Imaging. 2016; 43:2183–2189. [PubMed: 27349245]
9. De Vis JB, Petersen ET, Alderliesten T, et al. Non-invasive MRI measurements of venous oxygenation, oxygen extraction fraction and oxygen consumption in neonates. Neuroimage. 2014; 95:185–192. [PubMed: 24685437]
10. Thorngren-Jerneck K, Ohlsson T, Sandell A, et al. Cerebral Glucose Metabolism Measured by Positron Emission Tomography in Term Newborn Infants with Hypoxic Ischemic Encephalopathy. Pediatr Res. 2001; 49:495–501. [PubMed: 11264432]
11. Mintun MA, Raichle ME, Martin WR, Herscovitch P. Brain oxygen utilization measured with O-15 radiotracers and positron emission tomography. J Nucl Med. 1984; 25:177–87. [PubMed: 6610032]
12. Lu H, Ge Y. Quantitative evaluation of oxygenation in venous vessels using T2-Relaxation-Under-Spin-Tagging MRI. Magn Reson Med. 2008; 60:357–363. [PubMed: 18666116]
13. Petersen ET, De Vis JB, Alderliesten T, et al. Simultaneous OEF and hematocrit assessment using T2 prepared blood relaxation imaging with inversion recovery. Proc Int Soc Magn Reson Med. 20:472.
14. Jain V, Langham MC, Wehrli FW. MRI estimation of global brain oxygen consumption rate. J Cereb Blood Flow Metab. 2010; 30:1598–607. [PubMed: 20407465]
15. An H, Lin W. Quantitative measurements of cerebral blood oxygen saturation using magnetic resonance imaging. J Cereb Blood Flow Metab. 2000; 20:1225–36. [PubMed: 10950383]
16. De Vis JB, Hendrikse J, Bhogal A, Adams A, Kappelle LJ, Petersen ET. Age-related changes in brain hemodynamics; A calibrated MRI study. Hum Brain Mapp. 2015; 36:3973–3987. [PubMed: 26177724]
17. Zhang J, Liu T, Gupta A, Spincemaille P, Nguyen TD, Wang Y. Quantitative mapping of cerebral metabolic rate of oxygen ($CMRO_2$) using quantitative susceptibility mapping (QSM). Magn Reson Med. 2015; 74:945–52. [PubMed: 25263499]

18. ElSankari S, Balédent O, van Pesch V, Sindic C, de Broqueville Q, Duprez T. Concomitant analysis of arterial, venous, and CSF flows using phase-contrast MRI: a quantitative comparison between MS patients and healthy controls. J Cereb Blood Flow Metab. 2013; 33:1314–21. [PubMed: 23778162]
19. Schuchardt F, Schroeder L, Anastasopoulos C, et al. In vivo analysis of physiological 3D blood flow of cerebral veins. Eur Radiol. 2015; 25:2371–80. [PubMed: 25638218]
20. Xu F, Liu P, Pascual JM, Xiao G, Lu H. Effect of hypoxia and hyperoxia on cerebral blood flow, blood oxygenation, and oxidative metabolism. J Cereb Blood Flow Metab. 2012; 32:1909–18. [PubMed: 22739621]
21. Chen JJ, Pike GB. Global cerebral oxidative metabolism during hypercapnia and hypocapnia in humans: implications for BOLD fMRI. J Cereb Blood Flow Metab. 2010; 30:1094–9. [PubMed: 20372169]
22. Lu H, Liu P, Yezhuvath U, Cheng Y, Marshall O, Ge Y. MRI mapping of cerebrovascular reactivity via gas inhalation challenges. J Vis Exp. Jan.2014 Epub ahead of print. doi: 10.3791/52306
23. Lu H, Xu F, Grgac K, Liu P, Qin Q, van Zijl P. Calibration and validation of TRUST MRI for the estimation of cerebral blood oxygenation. Magn Reson Med. 2012; 67:42–9. [PubMed: 21590721]
24. Lu H, Clingman C, Golay X, van Zijl PC. Determining the longitudinal relaxation time (T1) of blood at 3.0 Tesla. Magn Reson Med. 2004; 52:679–82. [PubMed: 15334591]
25. Xu F, Uh J, Liu P, Lu H. On improving the speed and reliability of T2-relaxation-under-spin-tagging (TRUST) MRI. Magn Reson Med. 2012; 68:198–204. [PubMed: 22127845]
26. Evans AJ, Iwai F, Grist TA, et al. Magnetic resonance imaging of blood flow with a phase subtraction technique. In vitro and in vivo validation. Invest Radiol. 1993; 28:109–15. [PubMed: 8444566]
27. Peng S-L, Su P, Wang F-N, et al. Optimization of phase-contrast MRI for the quantification of whole-brain cerebral blood flow. J Magn Reson Imaging. 2015; 42:1126–33. [PubMed: 25676350]
28. Liu P, Xu F, Lu H. Test-retest reproducibility of a rapid method to measure brain oxygen metabolism. Magn Reson Med. 2013; 69:675–81. [PubMed: 22517498]
29. Peng SL, Dumas JA, Park DC, et al. Age-related increase of resting metabolic rate in the human brain. Neuroimage. 2014; 98:176–83. [PubMed: 24814209]
30. Lotz J, Meier C, Leppert A, Galanski M. Cardiovascular flow measurement with phase-contrast MR imaging: basic facts and implementation. Radiographics. 22:651–71.
31. Bland JM, Altman DG. Statistical methods for assessing agreement between two methods of clinical measurement. Lancet. 1986; 1:307–10. [PubMed: 2868172]
32. Kuroda S, Houkin K, Ishikawa T, Nakayama N, Iwasaki Y. Novel bypass surgery for moyamoya disease using pericranial flap: its impacts on cerebral hemodynamics and long-term outcome. Neurosurgery. 2010; 66:1093–101. [PubMed: 20495424]
33. Jain V, Magland J, Langham M, Wehrli FW. High temporal resolution in vivo blood oximetry via projection-based T2 measurement. Magn Reson Med. 2013; 70:785–90. [PubMed: 23081759]
34. Krishnamurthy LC, Mao D, King KS, Lu H. Correction and optimization of a T2-based approach to map blood oxygenation in small cerebral veins. Magn Reson Med. 2016; 75:1100–9. [PubMed: 25846113]
35. Sethi SK, Utriainen DT, Daugherty AM, et al. Jugular Venous Flow Abnormalities in Multiple Sclerosis Patients Compared to Normal Controls. J Neuroimaging. 25:600–7.
36. Louveau A, Smirnov I, Keyes TJ, et al. Structural and functional features of central nervous system lymphatic vessels. Nature. 2015; 523:337–41. [PubMed: 26030524]
37. Rasulo FA, Bertuetti R, Robba C, et al. The accuracy of transcranial Doppler in excluding intracranial hypertension following acute brain injury: a multicenter prospective pilot study. Crit Care. 2017; 21:44. [PubMed: 28241847]
38. Doshi H, Wiseman N, Liu J, et al. Cerebral Hemodynamic Changes of Mild Traumatic Brain Injury at the Acute Stage. PLoS One. 2015; 10:e0118061. [PubMed: 25659079]
39. Kim ESH, Diaconu C, Baus L, et al. Chronic cerebrospinal venous insufficiency: pitfalls and perils of sonographic assessment. J Ultrasound Med. 2015; 34:1097–106. [PubMed: 26014330]

40. Schrauben EM, Anderson AG, Johnson KM, Wieben O. Respiratory-induced venous blood flow effects using flexible retrospective double-gating. J Magn Reson Imaging. 2015; 42:211–6. [PubMed: 25210850]

41. Diaconu CI, Fox RJ, Grattan A, et al. Hydration status substantially affects chronic cerebrospinal venous insufficiency assessments. Neurol Clin Pract. 2013; 3:386–391. [PubMed: 24175155]

42. Faull OK, Cotter JD, Lucas SJE. Cerebrovascular responses during rowing: Do circadian rhythms explain morning and afternoon performance differences? Scand J Med Sci Sports. 2015; 25:467–75. [PubMed: 24942089]

43. Bulte DP, Chiarelli PA, Wise RG, Jezzard P. Cerebral perfusion response to hyperoxia. J Cereb Blood Flow Metab. 2007; 27:69–75. [PubMed: 16670698]

44. Xu F, Liu P, Pascual JM, Xiao G, Lu H. Effect of hypoxia and hyperoxia on cerebral blood flow, blood oxygenation and oxidative metabolism. J Cereb Blood Flow Metab. 2012; 32:1909–18. [PubMed: 22739621]

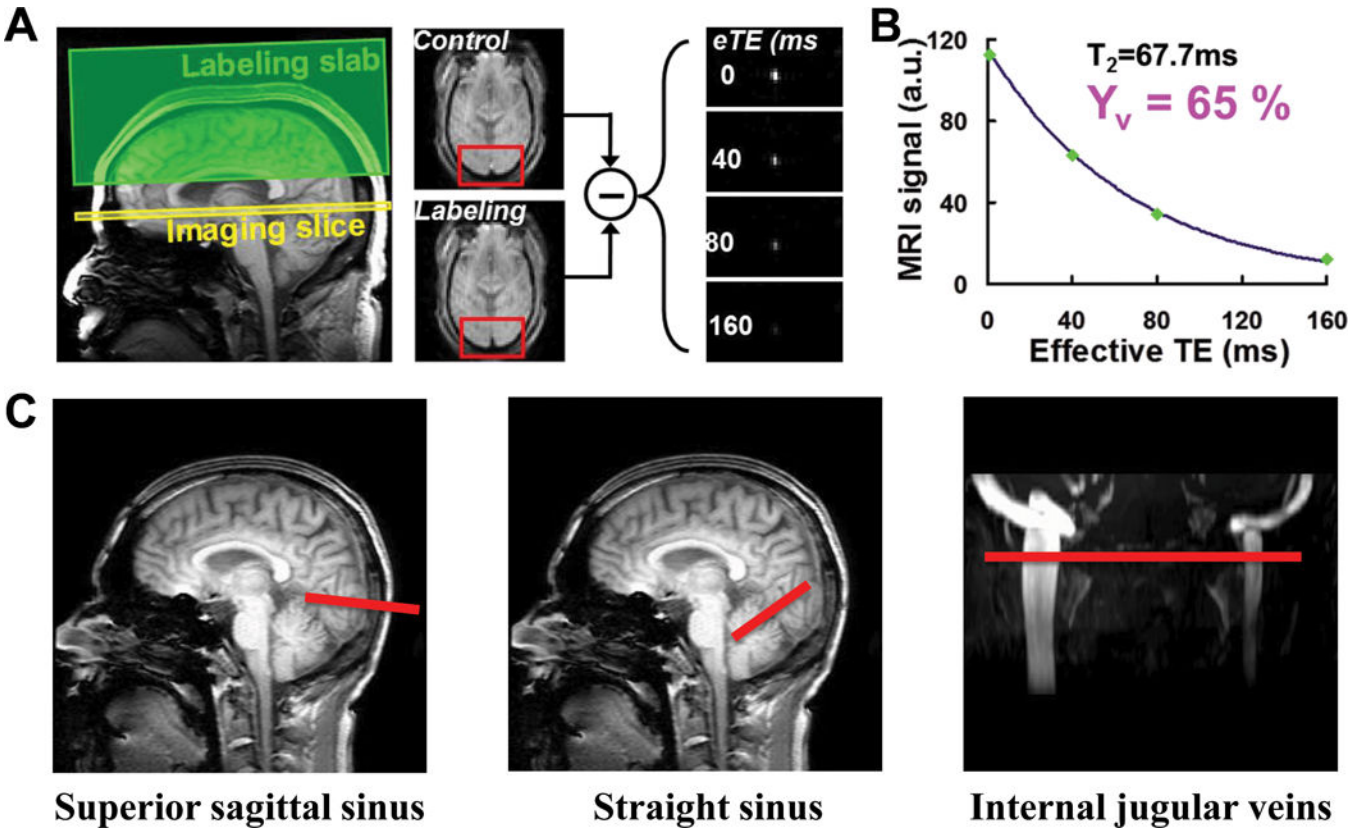

Figure 1.

Illustration of the TRUST MRI technique and the position of the imaging slices on the venous sinuses. (A) Demonstration of the labeling (green) and imaging (yellow) slab of the TRUST MRI sequence, in which the imaging slab is positioned perpendicular to the superior sagittal sinus (SSS). An example of a control and a label image is given; note the different signal intensities in the SSS caused by the inversion pulse applied to achieve the labeling. (B) Plot of the venous blood signal obtained over different effective echo times (eTE of 0,40, 80, and 160ms). Monoexponential fitting of the signal decay provides the T_2 value of the venous blood from which the venous oxygenation is obtained. (c) Positioning of the imaging slices (red lines) on the venous sinuses for TRUST MRI.

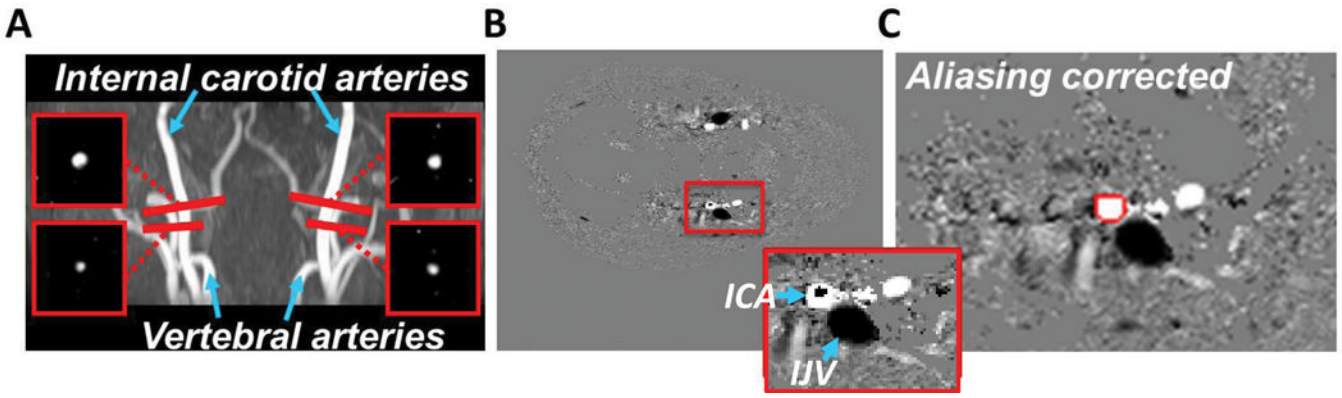

Figure 2.

Illustration of the positioning of the PC MR imaging slices on the feeding arteries, and example images of the postprocessing of the PC MR images. (A) To obtain whole-brain blood flow, flow within the internal carotid arteries and within the vertebral arteries was measured and enumerated. (B) Blood flow with a velocity higher than the velocity encoding (typically in the center of the vessel) causes phase wrapping for which velocity aliasing correction was performed. Figure inset shows the zoomed-in view of the red box, where the dark spot inside the internal carotid artery (ICA) represent an example of phase wrapping. The internal jugular vein (IJV) appeared dark because of its opposite flow direction. (C) On the aliasing-corrected images, the flow was measured by manually delineating the vessel (red line).

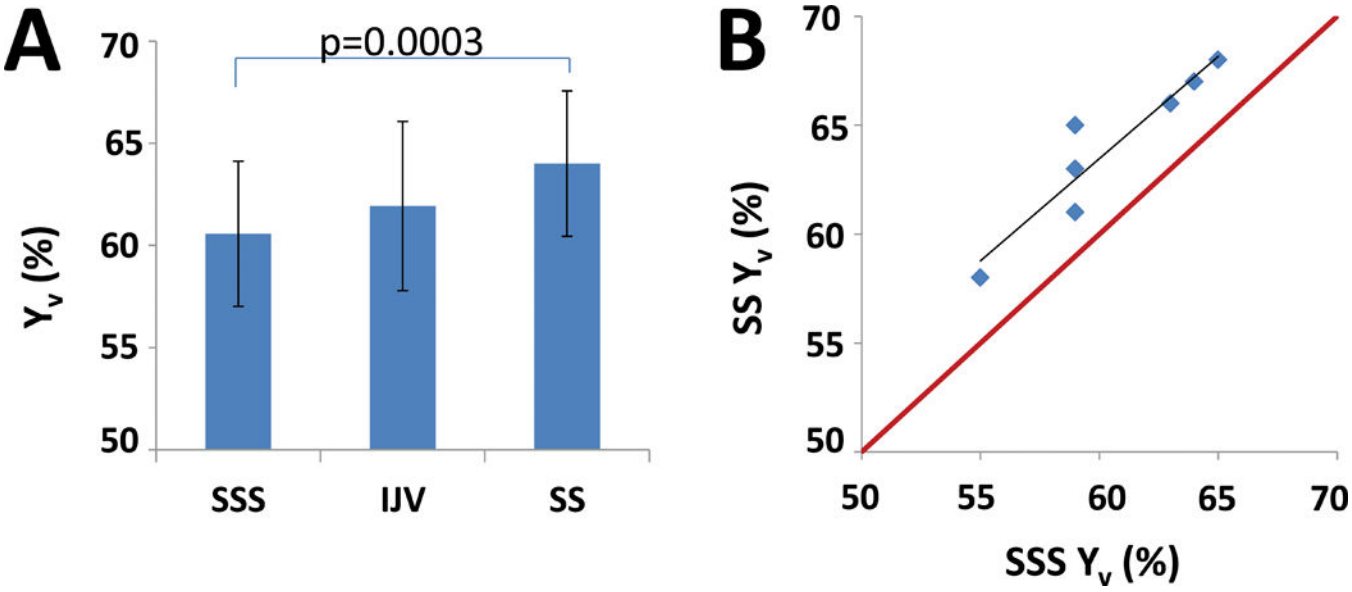

Figure 3.

Results of the venous oxygenation measurements. (A) Y_v at the major veins. (B) Scatterplot between the SSS-Y_v and the SS-Y_v. Red line indicates unity line. Black line indicates the linear regression.

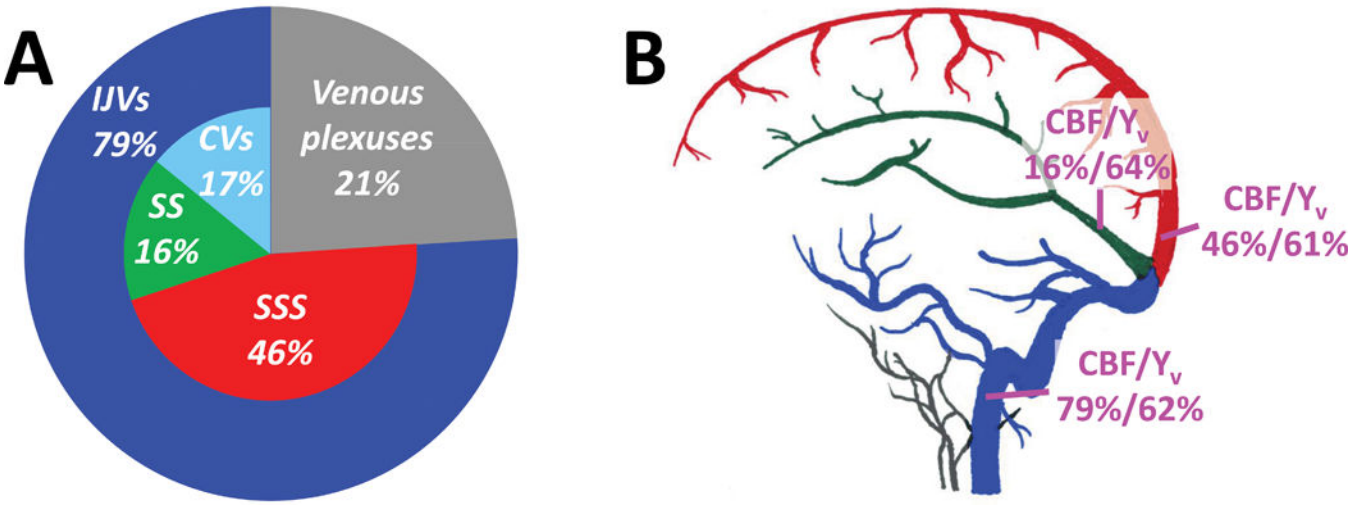

Figure 4.

Results of the blood flow measurements. (A) Pie plot of the venous blood distribution. (B) Illustration of the blood flow (normalized by whole-brain blood flow) and oxygenation (in units of the oxygen saturation fraction) in the three major drainage veins. SSS, superior sagittal sinus; SS, straight sinus; CVs, cerebellar veins; IJVs, internal jugular veins.

Table 1

Velocity encoding for PC MRI across vessels

Vessel	V_{enc} at baseline breathing (in cm/s)	V_{enc} at hypercapnic breathing (in cm/s)
ICA	40	60
VA	30	45
SSS	40	60
SS	30	45
IJV	40	60

ICA, internal carotid artery; VA, vertebral artery; SSS, superior sagittal sinus; SS, straight sinus; IJV, internal jugular vein; V_{enc}, velocity encoding.

Table 2

EtO_2 and $EtCO_2$ values under various breathing conditions.

	EtO_2 (mmHg)	**$EtCO_2$ (mmHg)**	**ΔEtO_2 (mmHg)**	**$\Delta EtCO_2$ (mmHg)**
Baseline	98±7	45±4	–	–
Hyperoxia	655±22	41±2	558±23	–
Hypercapnia	126±5	53±3	–	9±2

EtO_2, end-tidal O_2; $EtCO_2$, end-tidal CO_2.

Table 3

Blood flow at baseline and hypercapnia

	AI (ml/min)	SSS (ml/min)	SS (ml/min)	SSS + SS (ml/min)	IJVs (ml/min)
Baseline	772 ± 181	362 ± 143	124 ± 33	486 ± 160	623 ± 234
HC	1095 ± 208	552 ± 189	172 ± 49	724 ± 227	908 ± 287
ΔHC	42%	52%	39%	49%	46%

HC, hypercapnia; ΔHC, the percentage flow change from baseline to hypercapnia; AI, arterial inflow, flow through the four brain feeding arteries; SSS, superior sagittal sinus; SS, straight sinus; IJVs, internal jugular veins.